Article

Carbon-sink potential of continuous alfalfa agriculture lowered by short-term nitrous oxide emission events

Tyler L. Anthony [1] ✉, Daphne J. Szutu[1], Joseph G. Verfaillie [1], Dennis D. Baldocchi [1] & Whendee L. Silver [1]

Alfalfa is the most widely grown forage crop worldwide and is thought to be a significant carbon sink due to high productivity, extensive root systems, and nitrogen-fixation. However, these conditions may increase nitrous oxide (N_2O) emissions thus lowering the climate change mitigation potential. We used a suite of long-term automated instrumentation and satellite imagery to quantify patterns and drivers of greenhouse gas fluxes in a continuous alfalfa agroecosystem in California. We show that this continuous alfalfa system was a large N_2O source (624 ± 28 mg N_2O m^2 y^{-1}), offsetting the ecosystem carbon (carbon dioxide (CO_2) and methane (CH_4)) sink by up to 14% annually. Short-term N_2O emissions events (i.e., hot moments) accounted for ≤1% of measurements but up to 57% of annual emissions. Seasonal and daily trends in rainfall and irrigation were the primary drivers of hot moments of N_2O emissions. Significant coherence between satellite-derived photosynthetic activity and N_2O fluxes suggested plant activity was an important driver of background emissions. Combined data show annual N_2O emissions can significantly lower the carbon-sink potential of continuous alfalfa agriculture.

Alfalfa (*Medicago sativa*), a nitrogen (N) fixing species, is the most widely grown perennial forage crop worldwide and the largest crop by land area in the Western United States[1,2]. Alfalfa is traditionally used as cattle feed and growth in alfalfa land area is largely driven by increasing global feed demand for dairy and other livestock production[3]. Soil N inputs from symbiotic N fixation[4] help support plant growth but may also be a source of nitrous oxide (N_2O) emissions from both nitrification and denitrification[5]. From a carbon (C) accounting perspective, alfalfa has been referred to as a climate-friendly feedstock due to its soil C sequestration potential as a deep-rooting, perennial plant and reduced N fertilizer inputs[6]. However, few studies have combined carbon dioxide (CO_2), methane (CH_4), and N_2O fluxes in the total net annual CO_2-equivalent (CO_2e) budgets of alfalfa agroecosystems. Continuous measurements are needed to assess the greenhouse gas emissions and net C balance of continuous alfalfa ecosystems as these

are likely to differ from other agriculture practices that incorporate alfalfa in short-term rotations[7–9].

The biogeochemical processes that drive N_2O production are notorious for being temporally dynamic and characterized by hot moments of emissions, defined as short periods in time with fluxes significantly larger than the mean[5,10,11]. Thus short-term or infrequent sampling is likely to underestimate the role of hot moments in annual N_2O fluxes[12]. Alfalfa typically has a high water demand and is often irrigated throughout the growing season to maintain productivity[13]. Short periods of anaerobiosis following irrigation or rainfall events combined with soil N inputs can create ideal conditions for hot moments of N_2O production. Acidic conditions may exacerbate the effect as N_2O reductase is inhibited at low pH[5,14]. Oxygen (O_2) availability is an important control on N_2O production via nitrification and anaerobic denitrification[5]. Nitrous oxide production can also be

[1]Ecosystem Science Division, Department of Environmental Science, Policy and Management, University of California at Berkeley, 130 Mulford Hall, Berkeley, CA 94720, USA. ✉e-mail: t.anthony@berkeley.edu

limited by temperature, substrate C, nitrate (NO_3^-), or ammonium (NH_4^+) availability[15]. In soils, these variables are likely regulated by nonlinear asynchronous processes across temporal scales[5,16], requiring high frequency measurements to effectively characterize the controls on N_2O hot moments, and determine drivers of background (i.e., non-hot moment) N_2O fluxes.

The global warming potential of alfalfa agriculture is also affected by carbon dioxide (CO_2) and methane (CH_4) fluxes. Both CO_2 and CH_4 fluxes may be characterized by hot moments of soil emissions. Increased CO_2 respiration often occurs following soil rewetting[17-20] and these pulses can contribute a significant fraction of the annual CO_2 release, particularly in water-limited systems[19,21]. Heterotrophic respiration is thought to be directly regulated by substrate availability, primarily plant photosynthate[22], which can also stimulate the production and emissions of N_2O and CH_4[23,24]. For example, root exudates are well-known labile soil C sources that can prime microbial activity and associated pulses in soil respiration[25]. Up to 20% of C fixed by photosynthesis is released by root exudation that may occur as pulsed inputs[26,27]. Changes in plant productivity within and across years may also regulate greenhouse gas fluxes through impacts on other photosynthetic inputs such as plant litter[28,29]. Alfalfa is generally a net CH_4 sink via microbial CH_4 oxidation under well-drained conditions[6,30,31], but high rainfall events and irrigation can produce anaerobic conditions that can stimulate hot moments of methanogenesis[32]. Even with the potential for periodic CH_4 emissions and CO_2 pulses, long-term eddy covariance measurements of CO_2 and CH_4 suggest that alfalfa cropping systems can be net C sinks at an ecosystem scale[6,31]. However, continuous N_2O measurements are needed to determine the total CO_2e of soils emissions from alfalfa.

With the increasing agricultural demand for alfalfa, continuous long-term measurements of greenhouse gas fluxes are needed to better quantify the net climate impacts of alfalfa agroecosystems. It is also critical to determine the drivers of greenhouse gas emissions to better manage alfalfa for emissions reduction. We used a combined suite of automated flux chambers, continuous environmental sensing, eddy covariance, and satellite imagery of photosynthetic activity to determine patterns and associated controls of CO_2, N_2O, and CH_4 fluxes over four complete years in irrigated alfalfa. We used continuous cavity ring-down spectroscopy (CRDS) and automated chambers to collect over 103,000 individual N_2O, CH_4, and CO_2 flux measurements which were coupled with soil O_2, moisture, and temperature sensors installed across the soil profile and a year-long intensive weekly sampling campaign for soil gas (CO_2, N_2O, and CH_4), mineral N, and soil pH. We tested the hypothesis that the combination of mineral N availability and low redox conditions are the primary drivers of hot moments of N_2O emissions and that hot moments offset a significant portion of the net CO_2e sink. We predicted that low redox conditions would occur during irrigation and high rainfall events, particularly during warm periods as the solubility of O_2 decreases with increasing temperature[33]. We also hypothesized that background patterns in N_2O emissions would follow patterns in plant activity indicative of the potential impact of plants on C or substrate availability.

Results and discussion
Annual soil N_2O budgets and ecosystem CO_2e balance
Annual mean N_2O fluxes were 624.4 ± 26.8 mg N_2O m^{-2} yr^{-1} (Table 1, range: 247.0 ± 5.7 to 901.9 ± 74.5 mg N_2O m^{-2} yr^{-1}) and were similar to or greater than other N_2O flux estimates from alfalfa systems[7,34-37]. However, few studies report flux measurements from irrigated, continuous alfalfa monocultures[36,37], which make up the majority of alfalfa ecosystems in the Western United States[2,7,13,38]. Annual soil N_2O emissions were highest in site years 2 and 3 (Table 1, $p < 0.001$) and lowest in site year 4 ($p < 0.001$). The use of N-fixing crops as a means to reduce N fertilizer inputs to agroecosystems is expected to decrease overall N_2O agricultural emissions[39]. However, the mean N_2O fluxes observed here

(4.0 ± 0.2 kg N-N_2O ha^{-1} y^{-1}) were equal to or higher than rates from fertilized agricultural ecosystems[40,41]. This suggests net N_2O emissions from irrigated alfalfa may not always be reduced relative to other agricultural ecosystems receiving inorganic N inputs, particularly on relatively C-rich soils.

Soil N_2O fluxes reduced the annual net CO_2e sink (sum of eddy covariance NEE and chamber N_2O and CH_4; Table 1) by up to 14% (mean: $8 \pm 0.4\%$). The ecosystem was a consistent net CO_2e sink (mean: -450.4 ± 121.9 g CO_2e m^{-2} y^{-1}) when estimated using eddy covariance NEE observations and chamber observations of N_2O and CH_4 (Table 1). Annual global warming potential (GWP) values were significantly greater in years 3 and 4 than years 1 and 2, driven by significant increases in net ecosystem exchange (NEE) and lower N_2O fluxes in year 4 (Table 1). Annual CH_4 fluxes were a consistent CO_2e sink (mean: -1.5 ± 0.1 g CO_2e m^{-2} y^{-1}) but were always less than 0.5% of the annual net GWP.

The importance of N_2O hot moments
Inter- and intra-annual variability in N_2O fluxes were largely driven by differences in the magnitude and frequency of hot moments of N_2O production. Hot moments represented only 0.2 to 1.1% of annual N_2O measurements but contributed up to 57% (mean: $44.4 \pm 6.3\%$) of total N_2O emissions (Table 2), highlighting the importance of continuous measurements for capturing high emission events and that continuous background fluxes (i.e., lower than hot moments) still represent a significant portion of the annual budget. The magnitude of hot moments decreased with stand age, and the contribution of hot moments to the annual flux also decreased over time (Fig. 1c, Table 2, $p < 0.001$). The decrease in the magnitude of hot moments of N_2O emissions over time may be partially explained by increased alfalfa taproot development with stand age. Nitrous oxide fluxes are generally expected to increase with alfalfa stand age[36], driven by increasing organic matter and N inputs from more developed root systems. However, irrigation frequency is likely to decrease in more established stands or in systems supported by subsurface irrigation or a shallow water table[42-44], which could lower N_2O fluxes[45]. A well-developed taproot system can maintain access to a deep-water table to support plant water demands, reducing drought stress[46,47] and the need for irrigation events that stimulate hot moments of N_2O emissions. The decreased contribution and magnitude of N_2O hot moments did not consistently correspond to decreases in annual emissions (Table 2). This may be due to increases in N_2O emissions associated with the accumulation and mineralization of residual alfalfa-derived organic matter[36]. Here we found that reduced irrigation frequency drove the observed decreases in hot moment emissions with stand age. However, these emissions reductions were partially offset by background (i.e., lower than hot moment) increases in N_2O production, which could have been derived from greater soil C and N availability.

Drivers of soil N_2O emissions
Acidic soil conditions were maintained throughout the year (Fig. 2c), creating a favorable pH environment for incomplete denitrification following decreases in soil O_2 availability[48]. These soils were relatively C-rich (5% soil C from 0–30 cm)[49], which may have also contributed to the higher observed N_2O emissions here[50], but newly mineralized alfalfa roots and shoots were likely an important soil NO_3^- source[51] and substrate for denitrification. We found that hot moments of N_2O production occurred following rapid increases in moisture and decreases in soil O_2 in warm surface soils; lower soil temperatures in winter appeared to limit hot moments of N_2O emission following rain events (Fig. 2). Summer hourly mean N_2O fluxes peaked in late afternoon (Fig. 3c, $p = 0.06$), within hours after the onset of irrigation events. However, short periods of irrigation did not always correspond to increased soil moisture at depths below 10 cm (Fig. 2). This could

Table 1 | Annual greenhouse gas emissions

Year	N$_2$O flux (mg N$_2$O m^{-2} y^{-1})	N$_2$O GWP (g CO$_2$e m^{-2} y^{-1})	CH$_4$ flux (mg CH$_4$ m^{-2} y^{-1})	CH$_4$ GWP (g CO$_2$e m^{-2} y^{-1})	Chamber CO$_2$ flux (g CO$_2$ m^{-2} y^{-1})	NEE (g CO$_2$ m^{-2} y^{-1})	Total CO$_2$e (g CO$_2$ m^{-2} y^{-1})	Eddy R$_{eco}$ (g CO$_2$ m^{-2} y^{-1})	Eddy GPP (g CO$_2$ m^{-2} y^{-1})
1 (2017–2018)	610.5 ± 68.1 a	181.9 ± 20.3 a	−44.0 ± 2.2 ab	−1.2 ± 0.1 ab	5869.5 ± 31.4 a	−1757 ± 85 a	−1576.3 ± 105.4 a	6485 ± 25 a	8242 ± 96 a
2 (2018–2019)	901.9 ± 74.5 b	268.8 ± 22.2 b	−31.6 ± 2.5 a	−0.9 ± 0.1 a	4135.0 ± 25.4 d	−1989 ± 86 a	−1721.1 ± 108.3 a	6141 ± 22 b	8129 ± 96 a
3 (2019–2020)	777.1 ± 52.0 ab	231.6 ± 15.5 ab	−60.6 ± 2.8 b	−1.7 ± 0.1 b	5217.3 ± 23.9 b	−2942 ± 101 b	−2712.1 ± 116.6 b	6513 ± 27 a	9455 ± 113 b
4 (2020–2021)	263.6. ± 5.6 c	78.6 ± 1.7 c	−78.2 ± 8.8 c	−2.2 ± 0.2 c	4565.2 ± 26.5 c	−2632 ± 93 b	−2555.6 ± 94.9 b	6521 ± 24 a	9153 ± 103 b
All	624.4 ± 27.8	186.1 ± 8.3	−53.5 ± 2.5	−1.5 ± 0.1	4925.9 ± 13.5	−2330 ± 46	−2115.4 ± 54.4	6451 ± 12	8745 ± 51

Mean (± standard error) annual chamber nitrous oxide (N$_2$O), methane (CH$_4$), and carbon dioxide (CO$_2$) fluxes, 100-year global warming potential (GWP) of N$_2$O and CH$_4$ in CO$_2$-equivalence (CO$_2$e), eddy covariance annual mean net ecosystem exchange (NEE), and annual field-scale CO$_2$e emissions (combination of chamber N$_2$O and CH$_4$ fluxes and eddy covariance NEE) by site year. Net ecosystem exchange (NEE) was derived from ecosystem respiration (R$_{eco}$) and gross primary productivity (GPP) eddy-covariance measurements. Letters denote statistically significant differences among annual values ($p < 0.01$) with statistical results reported from one-way repeated measures ANOVAs.

Table 2 | N$_2$O fluxes

Year	Annual mean (mg N$_2$O m^{-2} y^{-1})	Flux (n)	Hot moment flux (n)	Hot moment mean (mg N$_2$O m^{-2} d^{-1})	Hot moments removed mean (mg N$_2$O m^{-2} y^{-1})	Hot moments % of total flux
1 (2017–2018)	610.5 ± 68.1	25,252	48	496.1 ± 66.8	263.4 ± 9.9	56.8%
2 (2018–2019)	901.9 ± 74.5	25,169	74	456.6 ± 43.0	402.4 ± 13.7	55.3%
3 (2019–2020)	777.1 ± 52.0	26,261	55	363.1 ± 46.2	485.7 ± 10.4	37.5%
4 (2020–2021)	263.6 ± 5.6	25,336	273	19.8 ± 0.7	180.39 ± 2.6	31.6%
All years	624.4 ± 27.8	103,013	201	401.1 ± 26.9	346.9 ± 4.7	44.4%

Mean (± standard error) annual nitrous oxide (N$_2$O) fluxes by site year, number of measurements, number of outlier measurements, outlier mean (± standard error) N$_2$O fluxes, mean N$_2$O fluxes (± standard error) without hot moments included, and contribution of hot moments to total mean flux. Hot moments were calculated separately for each year and in aggregate for the total dataset (All years).

indicate that the majority of N$_2$O production during hot moments occurred near the soil surface.

Soil N$_2$O fluxes were significantly greater in the summer and lowest in the fall (Fig. 3c, $p < 0.001$). Seasonal and diel trends in soil N$_2$O fluxes further emphasized the importance of soil moisture changes from irrigation and rainfall events. Mean hourly N$_2$O fluxes during summer periods, when most irrigation events occurred, were consistently greater than any other period (Fig. 3c, $p < 0.001$). Overall, daily mean N$_2$O fluxes were positively correlated with weekly soil atmosphere N$_2$O concentrations across depths, suggesting N$_2$O production across the soil profile contributed to background soil N$_2$O emissions (Supplementary Information, Fig. S1, 10 cm R^2 = 0.60, $p < 0.001$, 30 cm R^2 = 0.53, $p < 0.001$, 50 cm R^2 = 0.45, $p < 0.001$). Temporal patterns in soil moisture, soil temperature, and bulk soil O$_2$ concentrations covaried across all depths and were significantly related to patterns in net N$_2$O fluxes on a daily timescale (Fig. S2, $p < 0.05$). Primary interactions between N$_2$O and moisture, temperature, and O$_2$ suggested that changes in N$_2$O fluxes were generally in phase but lagged changes in these variables at daily and weekly timescales (Supplementary Information, Fig. S2, $p < 0.05$). At weekly and monthly timescales, N$_2$O fluxes were predominantly associated with soil temperature and moisture at 10 and 30 cm depths (Supplementary Information, Fig. S2, $p < 0.05$). Wavelet coherence analyses suggested that short-term, hot moments of N$_2$O emissions were stimulated by changes in moisture and O$_2$ concentrations in surface soils, as well as sustained acidic soil conditions. Acidic soil pH (Fig. 3) and lagged responses of temperature and moisture were the predominant controls at longer timescales (Supplementary Information, Fig. S2, $p < 0.05$).

Continuous low-magnitude N$_2$O production was an increasing fraction of total N$_2$O emissions over time (Table 2). In contrast to hot moments, consistent low magnitude N$_2$O fluxes were regulated by plant activity, soil moisture, and soil temperature throughout the soil profile. Increases in background (low magnitude) N$_2$O emissions were positively correlated with periods of high gross primary productivity (GPP), measured with satellite observations of near-infrared reflectance of vegetation (NIRv, Supplementary Information, Fig. S3, $p < 0.05$)[28]. Alfalfa releases a small proportion of its symbiotically-fixed N as NH$_4^+$ to the soil[52–54], and decreases in photosynthate supply to root nodules and exudates following shoot harvest may also limit C substrate availability to nitrifiers and denitrifiers[55]. While no relationships were observed between soil NO$_3^-$ or NH$_4^+$ and N$_2$O emissions during our weekly sampling campaign (Fig. 2b, Supplementary Information), observed coherence at a daily timescale between NIRv and N$_2$O suggested plant-derived C or NH$_4^+$ availability may regulate low magnitude N$_2$O emissions. Plants likely shifted C and N allocation to new plant growth immediately after cutting, leading to lower soil N$_2$O emissions. Emissions increased over the growing season, possibly due to greater root exudation as aboveground plant biomass re-established.

Soil CH$_4$ emissions

Soils were a small consistent net sink of CH$_4$, accounting for only 0.06% of the total net C based-CO$_2$e uptake over the four year period. Annual mean soil CH$_4$ fluxes were −53.5 ± 2.5 mg CH$_4$ m^{-2} y^{-1} (Table 1, range: −78.2 ± 8.8 to −31.6 ± 2.5 mg CH$_4$ m^{-2} yr^{-1}). The net CH$_4$ sink was significantly greater in site year 4 than all other years (Table 1, $p < 0.001$). Sinks measured here were larger than others alfalfa ecosystem estimates[10,31,56], likely from the lower detection limit of the CRDS and automated chambers. In contrast to expectations, decreases in bulk soil O$_2$ concentrations did not appear to drive significant increases in net CH$_4$ production or decreases in the CH$_4$ sink (Fig. 1). Extended periods of soil anaerobiosis may be required to stimulate net CH$_4$ production[12,57], and this was not observed during the four year measurement period. We did observe a substantial increase in soil CH$_4$ concentrations (but not surface fluxes) shortly following the largest decrease in soil O$_2$ concentrations in March and April 2019 (Fig. 1, Supplementary Information, Fig. S8). Elevated soil moisture may have limited gas diffusion. Slower diffusion together with methanotrophic consumption near the soil surface likely regulated net soil CH$_4$ efflux during this period[58,59]. We also observed significant variability in hourly mean diel CH$_4$ fluxes (Fig. 3d), but this
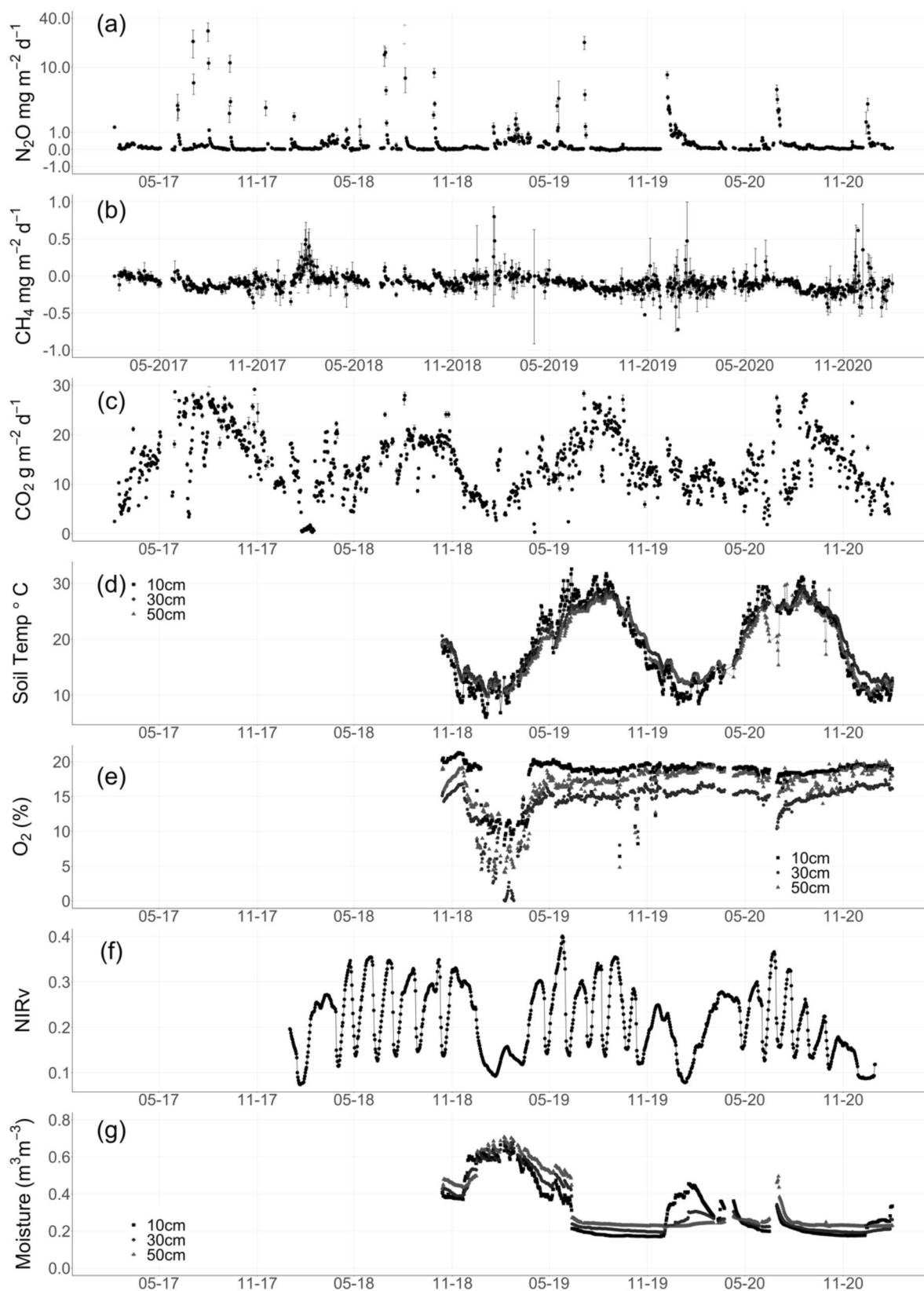
Fig. 1 | Greenhouse gas fluxes, soil sensing, and satellite imagery. Daily mean (± standard error) (**a**) carbon dioxide (g CO_2 m^{-2} d^{-1}), **b** methane (mg CH_4 m^{-2} d^{-1}), and **c** nitrous oxide (mg N_2O m^{-2} d^{-1}) fluxes (n = approximately 80 per day, with a total of 108,638, 103,013, and 102,997 flux measurements of CO_2, N_2O, and CH_4, respectively). Black circles represent mean daily flux measurements. Daily mean (± standard error) (**d**) soil temperature (°C), **e** soil oxygen (O_2), **f** daily near-infrared reflectance of vegetation (NIRv), and (**g**) volumetric soil moisture (m^3 m^{-3}) over the soil sensor measurement period and available daily satellite imagery (n = 96 measurements per day except for NIRv). For (**d**) soil temperature, (**e**) O_2, and (**g**) moisture, depth values are labeled as squares (10 cm), circles (30 cm), and triangles (50 cm).
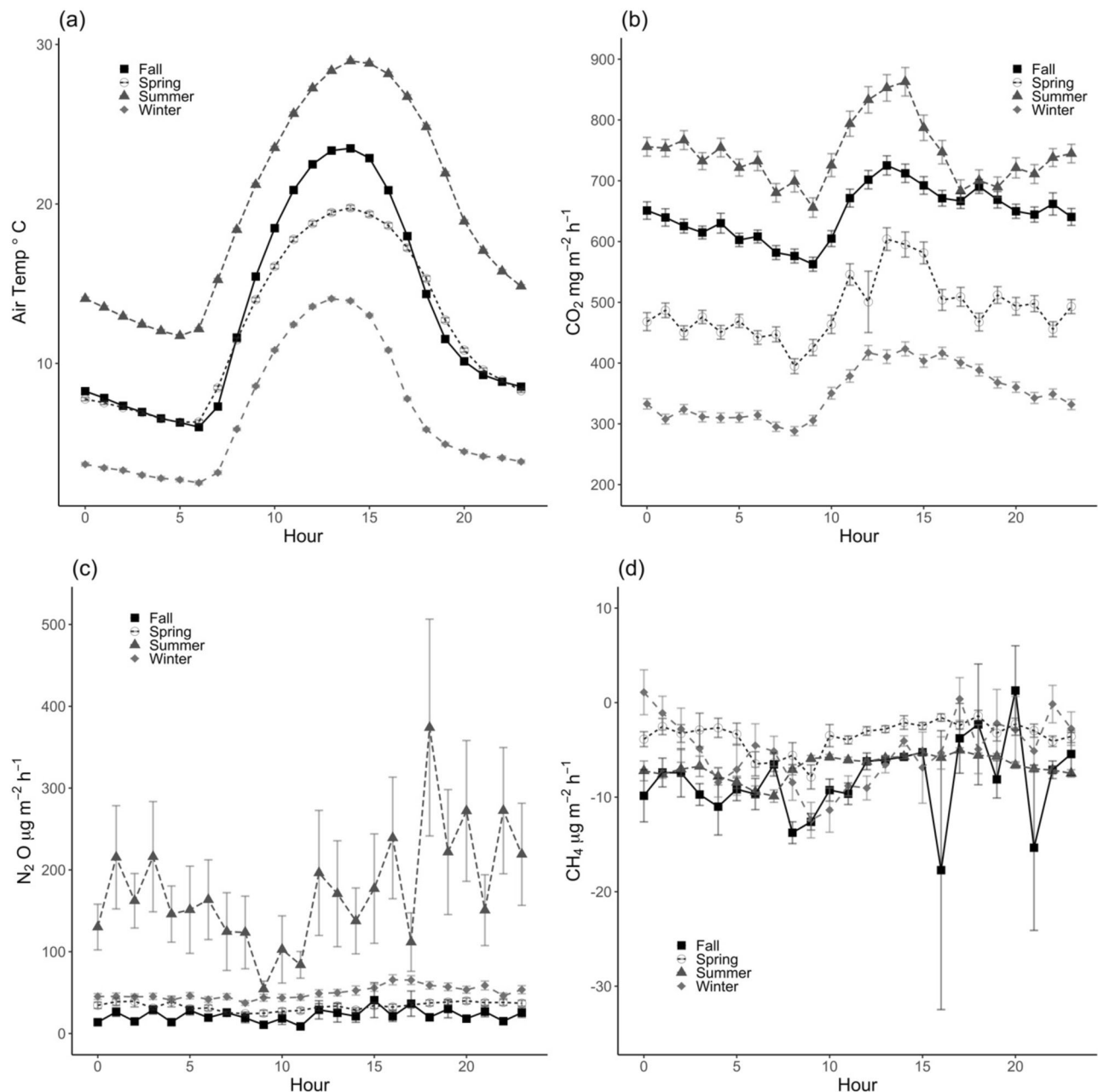
Fig. 2 | Diel greenhouse gas fluxes. Hourly mean (± standard error) (a) air temperature (°C), (**b**) carbon dioxide (CO_2) fluxes (mg CO_2 m^{-2} h^{-1}), (**c**) methane (CH_4) fluxes (µg CH_4 m^{-2} h^{-1}), and (**d**) nitrous oxide (N_2O) fluxes (µg N_2O m^{-2} h^{-1}), grouped by season (Fall = squares, Spring = open circles, Summer = triangles, and Winter = diamonds) over the entire measurement period (Fall: $n \geq 1220$ measurements per hour, Spring: $n \geq 848$ measurements per hour, Summer: $n \geq 956$ measurements per hour, Winter: $n \geq 1060$ measurements per hour).

variability was not significantly correlated with any measured soil characteristics.

Methane fluxes varied in response to temperature across depths and timescales and temperature was the strongest control on net CH_4 consumption (Supplementary Information, Fig. S4, $p < 0.05$). Decreases in soil moisture stimulated net CH_4 consumption (Supplementary Information, Fig. S4, $p < 0.05$), likely due to increased diffusivity[60,61] and O_2 availability. Periods of CH_4 uptake were highest in the late summer, occurring when soils were the driest throughout the soil profile (Fig. 1a, c). Lower soil moisture across the soil profile also generally corresponded to higher rates of CH_4 uptake and lower overall soil moisture increased CH_4 uptake with stand age, except for site year 2 (Table 1). Sustained CH_4 consumption combined with observed trends in N cycling suggest that CH_4 oxidation by nitrifiers

or nitrification by methanotrophs[62-65] could be regulating non-CO_2 greenhouse gas production and consumption under oxic conditions.

Agroecosystem CO_2 balance

Soil CO_2 emissions were greater than other alfalfa ecosystems[6], likely driven by a combination of high plant productivity, relatively high soil C content[49], and warm temperatures throughout the growing season. Chamber CO_2 fluxes, which here represent combined soil and root respiration, averaged 4925.9 ± 13.5 g CO_2 m^{-2} yr^{-1} and were lower than ecosystem respiration (R_{eco}) estimates (6451 ± 12 g CO_2 m^{-2} yr^{-1}) from the nearby eddy covariance observations (Table 1). Soil CO_2 fluxes closely followed seasonal patterns in soil temperature, with similar trends in soil temperature observed across depths (Fig. 1a, b). Surprisingly, soil CO_2 fluxes did not vary significantly with NIRv on
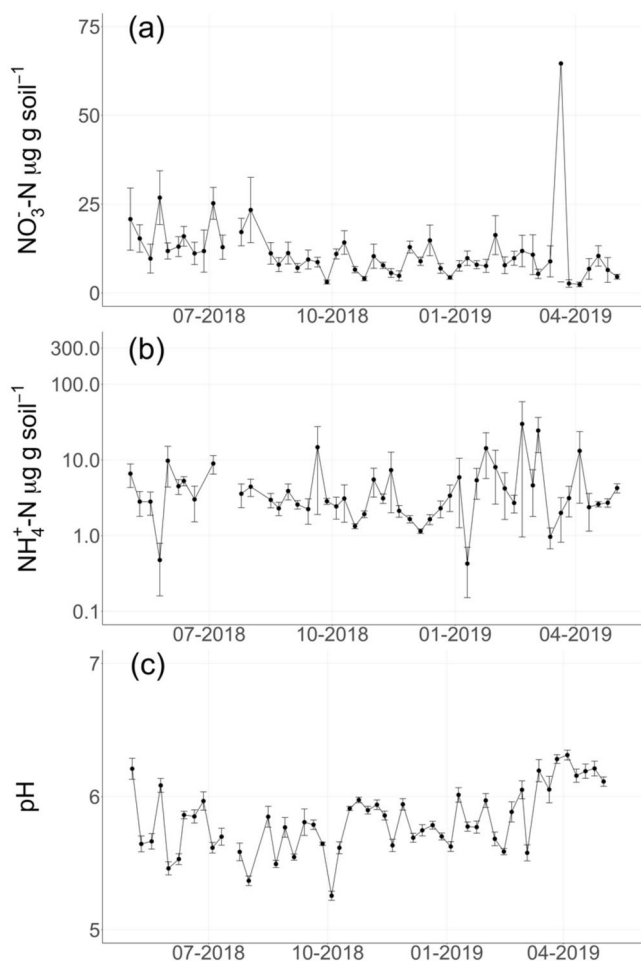
Fig. 3 | **Weekly soil nitrogen and pH.** Weekly mean (± standard error) (**a**) soil nitrate (µg NO_3^--N g soil^{-1}), **b** soil ammonium (µg NH_4^+-N g soil^{-1}), and **c** soil pH ($n = 10$ per week for 52 weeks). Manual soil measurements (0–10 cm depth) were conducted weekly from May 2018–May 2019.

Table 3 | Moisture, rainfall, and NIRv

Year	Mean 0-50 cm Soil Moisture (%)	Rainfall (mm y^{-1})	NIRv
1 (2017-2018)	–	444 a	–
2 (2018-2019)	47.8 ± 7.8 b*	356 ab	0.23 ± 0.01 a
3 (2019-2020)	35.3 ± 17.1 a	447 a	0.21 ± 0.01 b
4 (2020-2021)	24.3 ± 4.3 c	176 b	0.19 ± 0.01 c
All	31.5 ± 14	331 ± 64	0.21 ± 0.01

Annual mean (± standard error) 0–50 cm soil moisture ($n = 96$ measurements per day for 763 total days), annual rainfall (mm y^{-1}), and mean (± standard error) annual near-infrared reflectance of vegetation (NIRv) by site year (e.g., January 27 to January 26, $n = 365$ per year).
*Site year 2 soil moisture values include 5 out of 12 months. Letters denote significant differences between annual values ($p < 0.01$) with statistical results reported from one-way repeated measures ANOVAs.

within 5 to 7 days (Fig. 1a). Periods of increased plant growth rates following harvests likely resulted in a shift in C allocation from below- to aboveground[68] and highlights the importance of substrate limitation on NEE[29]. If aboveground regrowth increases plant nutrient demands, it could induce a lagged response in belowground respiration driven by subsequent reallocation of photosynthate belowground followed by enhanced soil nutrient mining by microbial communities[69]. The observed lagged relationships between NIRv and ecosystem greenhouse gas fluxes may also represent delays between photosynthetic CO_2 uptake and root C exudation processes. Short-term increases in soil moisture content and associated decreases in O_2 availability throughout the year were also important controls on soil respiration (Supplementary Information, Fig. S5, $p < 0.05$). Soil temperature across depths was significantly associated with respiration rates across timescales.

This combination of automated chambers, eddy covariance, soil sensing, and satellite imagery used here provided a comprehensive dataset of multi-year, annual, ecosystem-scale fluxes from a continuous alfalfa agroecosystem. We were able to determine the importance of both short-term hot moments and background emissions on total greenhouse gas budgets and explore scale-emergent drivers of N_2O emissions. We found that N_2O emissions reduced the net CO_2e sink at the ecosystem-scale by up to 14% annually and offset 70% of the ecosystem C sink after accounting for harvest biomass removal (post-harvest fate of harvested alfalfa was not included in this calculation). As hypothesized, this was predominantly driven by rare hot moments of soil N_2O emissions supplied by elevated soil NO_3^- pools and acidic soil conditions and stimulated by irrigation and rainfall events. Hot moments were ≤1% of measurements but averaged 44.4 ± 6.3% of annual N_2O fluxes. Additionally, background fluxes were likely driven by sustained substrate availability that varied with moisture, temperature, and NIRv, a possible index of plant inputs to soil. Lagged relationships between NIRv, CO_2, and N_2O fluxes suggested that plant inputs were likely an important driver of soil CO_2 fluxes and background N_2O emissions. Our results show that N_2O emissions likely significantly lower the field-scale C sink potential of this globally important crop. Hot moments of N_2O emissions, typically underestimated with traditional measurement approaches, played an outsized role in annual ecosystem-scale greenhouse gas budgets, highlighting the importance of continuous measurement for accurate ecosystem-scale greenhouse gas accounting.

Methods

Site info

The study was conducted in the Sacramento-San Joaquin Delta region of California, USA (38.11°N, 121.5°W). The site was in conventional perennial alfalfa (>5 years) that was periodically flood-irrigated during the growing season. The site was located on highly degraded

a daily scale (Supplementary Information, Fig. S3, $p < 0.05$). Soil CO_2 fluxes and NIRv covaried on weekly, monthly, and annual timescales highlighting the importance of plant harvesting and phenology in regulating soil respiration[28].

To quantify for C removed from the field, we used mean annual yields of 595 ± 137 g C m^{-2} y^{-1} or 2,072 ± 502 g CO_2 m^{-2} y^{-1} [31]. This is equivalent to 89% of NEE, with the remaining C (258.3 g CO_2 m^{-2} y^{-1} or 70.4 CO_2 m^{-2} y^{-1}) assumed to be stored as belowground biomass or soil C. With this number, the CO_2e of N_2O emissions would then offset 70% of the net CO_2 sink. The fate of harvested C was not considered in this study, which examined only ecosystem-scale fluxes. However, it should be noted that if conducting a life cycle analysis, harvested alfalfa is typically used as dairy or cattle feed, where alfalfa C is converted to a combination of both CO_2 and CH_4[66].

We observed significant differences in NIRv following alfalfa cutting events (Fig. 1c) and mean annual NIRv decreased significantly across the measurement period (Table 3, $p < 0.01$). Lags observed between NIRv and soil CO_2 fluxes may represent a delayed response to photosynthate availability as plants likely reallocate new photosynthate to aboveground biomass production following harvest events[67]. Alfalfa in this region can be harvested up to seven times per year, where the majority of aboveground plant biomass is removed[28,31]. Cuttings corresponded to significant reductions in mean daily soil respiration values, although soil respiration values typically recovered

peatland soils that have lost a significant proportion of their initial organic matter[49]. Alfalfa and corn are the dominant agricultural land uses in the region, with alfalfa representing 20% of agricultural land area (32,000 ha) in the Sacramento-San Joaquin Delta[70] and the largest crop by area in California (405,000 ha)[71]. Nearly 100% of alfalfa in California is irrigated, with flood irrigation being the most common practice[71]. The site had a Mediterranean climate with hot dry summers and cool wet winters. The region's historical mean annual temperature was $15.1 \pm 6.3\,°C$ and a mean annual rainfall averaging 326 ± 4 mm[23]. Site year (January 27 - January 26) rainfall data was collected from a nearby (<1 km) Ameriflux site[72]. Near-infrared reflectance of vegetation (NIRv), a metric for canopy photosynthetic activity[28], was calculated from daily 3 m resolution normalized difference vegetation index (NDVI) and near-infrared radiation (NIR) was collected from Planet Labs satellite imagery[73–75]. Near-infrared reflectance of vegetation was also used as a proxy for plant inputs to soils given that up to 20% of C fixed by photosynthesis is released by root exudation[26,27].

Ryde is the major soil series found under alfalfa in the region, and is widespread across the Sacramento San Joaquin-Delta and along the central coast of California[76]. Ryde soils belong to the fine-loamy, mixed, superactive, thermic Cumulic Endoaquolls taxonomic class and are very deep, poorly drained soils formed in alluvium from mixed rock sources and decomposed vegetative matter[76]. Total soil C concentrations (mean ± standard error) were $5.26 \pm 0.02\%$ at 0–15 cm, $5.00 \pm 0.15\%$ at 15–30 cm, and $1.99 \pm 0.09\%$ at 30–60 cm[49]. Total soil N concentrations were $0.38 \pm 0.003\%$ at 0–15 cm, $0.35 \pm 0.01\%$ at 15–30 cm, and $0.16 \pm 0.01\%$ at 30–60 cm[49].

Automated chamber measurements

Surface fluxes of N_2O, CH_4, and CO_2 were measured continuously from January 2017 to February 2021 using an automated chamber system. The system consisted of nine opaque, automated gas flux chambers (eosAC, Eosense, Nova Scotia, Canada) connected to a multiplexer (eosMX, Eosense, Nova Scotia, Canada). The multiplexer allowed for dynamically signaled chamber deployment and routed gases to a cavity ring-down spectrometer (Picarro G2508, Santa Clara, CA, USA). Chambers were measured sequentially over a 10-min sampling period with a 1.5-min flushing period before and after each measurement.

Chambers were deployed in a 10×10 m grid design, with each chamber approximately 5 m from other chambers. Extended 15 cm soil collars were utilized to maintain measurement collection and ensure chambers were not inundated during irrigation or high rainfall events. Chambers were randomly assigned to either plant rows ($n = 5$) or inter-plant areas of bare soil ($n = 4$). Chambers remained in their original positions throughout the field campaign, except for short periods (<3 days) during field management activities (e.g., harvest, winter grazing). Foliage near chambers were minimally trimmed as needed between harvests if it inhibited chamber closure.

To determine chamber volume, chamber collar heights were measured approximately weekly and interpolated between measurements to account for changes in chamber height over time. Chamber volumes were also used to calculate the minimum detectable flux of 0.002 nmol N_2O m^{-2} s^{-1}, 0.06 nmol CO_2 m^{-2} s^{-1}, and 0.002 nmol CH_4 m^{-2} s^{-1} [77]. The minimum detectable fluxes reported here are conservative estimates, as the actual chamber volume was always smaller than the maximum theoretical volume used to calculate these values.

Flux calculations and analyses were first performed using Eosense eosAnalyze-AC v. 3.7.7 software, then data quality assessment and control were subsequently performed in R (RStudio, v.1.1.4633)[78]. Fluxes were removed from the final dataset if they were associated with erroneous spectrometer cavity temperature or pressure readings or if any gas concentrations were negative, corresponding to instrument malfunction. Fluxes were also removed if the chamber

deployment period was less than 9 min or greater than 11 min, indicative of chamber malfunction. Calculated linear and exponential fluxes were compared using estimate uncertainty to estimate ratios, and in cases where both the linear and exponential models produced high uncertainty, the individual flux was eliminated from the dataset. Data filtering removed 2.1% of flux measurement periods, generating a final dataset of 108,638, 103,013, and 102,997 simultaneous flux measurements of CO_2, N_2O, and CH_4, respectively. Following data filtering, all statistical analyses were performed using JMP Pro 15 (SAS Institute Inc., Cary, NC). Differences in site year, hourly, and seasonal mean flux values were analyzed with one-way ANOVAs followed by post-hoc Tukey tests. Values reported in the text are means ± standard errors unless otherwise noted.

To quantify site-level CO_2 uptake[49] and calculate site-level global warming potential (GWP) we utilized annual net ecosystem exchange (NEE) estimates from a nearby (<1 km) Ameriflux tower[72] in alfalfa grown with identical management practices and soil type. Here we used the eddy covariance technique[79] to capture continuous, long-term exchange of CO_2, CH_4, H_2O, and energy fluxes between the landscape and the atmosphere, along with measurements of environmental drivers[80]. Fluxes were measured at a frequency of 20 Hz using open-path infrared gas analyzers (LI-7500 for CO_2 and H_2O, LI-7700 for CH_4, LiCOR Inc., Lincoln, NE, USA) that were calibrated at least every 6 months. Sonic anemometers measured sonic temperature and three-dimensional wind speed at 20 Hz (WindMaster Pro 1590, Gill Instruments Ltd, Lymington, Hampshire, England). To convert N_2O and CH_4 flux measurements to CO_2e, we used the IPCC AR5 100-year GWP values of 28 CO_2e for CH_4 and 298 CO_2e for N_2O[81].

Quantifying hot moments of greenhouse gas emissions

This large, continuous dataset allowed us to quantify N_2O hot moments and their impact on total N_2O emissions. Following data filtering, the quantity and magnitude of hot moment measurements and their impact on annual flux estimates were determined. We defined hot moments as flux measurements with values greater than four standard deviations from the mean[12], as statistically 99.9% of the population should fall within four standard deviations of the mean. Yearly mean flux values were then calculated for only hot moment fluxes, the entire flux dataset, and the flux dataset with hot moment observations removed to determine the impact of outlier fluxes on annual greenhouse gas emissions. Given our large and continuous dataset, we could also compare mean fluxes with and without high flux events[12,82] to better quantify the importance of hot moments.

Weekly soil measurements

Weekly soil samples (0–15 cm depth, $n = 10$ week^{-1}) were randomly collected with a 6 cm diameter soil auger within 30 m of the chamber array from April 2018 to May 2019. Soil samples were analyzed for gravimetric soil moisture, soil pH, and 2 M potassium chloride (KCl) extractable nitrate (NO_3^-) plus nitrite (NO_2^-) and ammonium (NH_4^+). For KCl extracts, we utilized a 5:1 ratio of 2 M KCl volume to oven dry equivalent (ODE) soil that were shaken for 1 h and subsequently filtered with Whatman Grade 1 filter paper[83]. The KCl extracts were then analyzed colorimetrically for NH_4^+ and NO_3^- using an AQ300 analyzer (Seal Instruments, Mequon, WI). Soil moisture was determined gravimetrically by drying 10 g of field-fresh soil to a constant weight at 105 °C. Soil pH was measured in a slurry of 10 g of field-fresh soil in 10 mL of distilled deionized water[84].

Soil sensor measurements

Two sets of soil sensors were installed from September 2018-February 2021 at depths of 10 cm, 30 cm, and 50 cm. This included SO-110 oxygen (O_2) and soil temperature sensors (Apogee Instruments,

Logan, UT) and CS616 moisture sensors (Campbell Scientific, Logan, UT) connected to a CR1000 datalogger (Campbell Scientific, Logan, UT) storing data at 15 min intervals. Sensors remained installed throughout the year. Erroneous data corresponding to sensor malfunction were removed from the dataset, which included 1.7% of soil moisture measurements and 3.4% of soil O_2 measurements. In total, there were 73 of 839 days missing during the soil sensor measurement period.

Weekly soil depth gas samples

Two replicate soil gas samples were taken for CO_2, CH_4, and N_2O at 10 cm, 30 cm, and 50 cm depths weekly from September 2018 to December 2019. Instrument grade stainless steel 1/8" tubing (Restek, Bellefonte, PA) was installed in parallel to the soil sensors above, with approximately 15 cm of tubing installed with multiple sampling holes parallel to the soil surface. Sampling septa (Restek, Bellefonte, PA) were installed in 1/8" Swagelok union (Swagelok, Solon, OH) permanently connected to the stainless-steel tubing. Septa were changed monthly. Gas samples were collected weekly with 30 ml BD syringes after first clearing the tubing dead volume. Short periods of soil inundation following extensive rainfall (March-April 2019) made it impossible to collect gas samples from some depths. Samples were stored in over-pressurized 20 ml glass vials with thick septa (Geomicrobial Technologies, Oechelata, OK) until manual sample injection analysis on a Shimadzu GC-34 (Shimadzu Corp., Tokyo, Japan). Generalized pairwise regression analyses were used to explore the relationships between measured soil atmosphere CO_2, CH_4, and N_2O concentrations and surface soil CO_2, CH_4, and N_2O fluxes.

Wavelet coherence analysis

Wavelet coherence analysis was used to identify interactions between soil greenhouse gas fluxes, NIRv, and the soil variables (O_2, moisture, and temperature at 10, 30, and 50 cm) measured[12,85,86]. Wavelet coherence is a tool for comparing time series and is used to determine significance, causality and scale-emergent interactions between variables[16,80,87]. Wavelet coherence measures the cross-correlation between time series and allowed us to explore relationships between greenhouse gas fluxes and potential controls of NIRv, O_2, moisture, and temperature at daily, monthly, and annual timescales. Wavelet coherence is derived from two time series as a function of decomposed frequency (Wave.xy) and the wavelet power spectrum (Power.x, Power.y) of each individual time series:

$$\text{Coherence} = \frac{|\text{Wave}.xy|^2}{\text{Power}.x \cdot \text{Power}.y} \tag{1}$$

This approach allows for continuous wavelet-based analysis of univariate and bivariate time series, facilitating comparisons of time series data across scales, leads, and lags[86,88]. Missing data were replaced with zeroes to compute an unbiased estimator of the wavelet variance for time series with missing observations[86,89]. Statistical significance (p-value) was computed using 1000 Monte Carlo simulations. All wavelet decomposition and coherence calculations were conducted using the WaveletComp 1.1 R package[88].

Reporting summary

Further information on research design is available in the Nature Portfolio Reporting Summary linked to this article.

Data availability

The daily mean greenhouse gas fluxes (chamber CO_2, CH_4, N_2O, and eddy covariance CO_2), satellite-derived vegetation indices (NIRv), soil gas concentrations, and soil O_2, temperature, and moisture sensor data generated in this study and used to create the figures have been deposited the Dryad database: https://doi.org/10.6078/D1ZQ53.

Code availability

The corresponding R code used in this study have been deposited in the Dryad database: https://doi.org/10.6078/D1ZQ53.

References

1. Yang, S. et al. Alfalfa benefits from Medicago truncatula: The RCT1 gene from M. truncatula confers broad-spectrum resistance to anthracnose in alfalfa. *Proc. Natl Acad. Sci. USA* **105**, 12164–12169 (2008).
2. Ottman, M. et al. Long term trends and the future of the alfalfa and forage industry. *Proc. 2013 Western Alfalfa & Forage Symposium, Reno, NV, 11-13, December, 2013. UC Cooperative Extension, Plant Sciences Department, University of California, Davis, CA 95616.* 11–13 (2013).
3. Wang, Q., Hansen, J. & Xu, F. China's emerging dairy markets and potential impacts on U.S. alfalfa and dairy product exports. *Clim. Change 2013 Phys. Sci. Basis* **53**, 1–30 (2013).
4. Peterson, T. A. & Russelle, M. P. Alfalfa and the nitrogen cycle in the Corn Belt. *J. Soil Water Conserv.* **46**, 229 LP–229235 (1991).
5. Butterbach-Bahl, K., Baggs, E. M., Dannenmann, M., Kiese, R. & Zechmeister-Boltenstern, S. Nitrous oxide emissions from soils: how well do we understand the processes and their controls? *Philos. Trans. R. Soc. Lond. B Biol. Sci.* **368**, 20130122 (2013).
6. Alberti, G. et al. Changes in CO2 emissions after crop conversion from continuous maize to alfalfa. *Agric. Ecosyst. Environ.* **136**, 139–147 (2010).
7. Tenuta, M., Amiro, B. D., Gao, X., Wagner-Riddle, C. & Gervais, M. Agricultural management practices and environmental drivers of nitrous oxide emissions over a decade for an annual and an annual-perennial crop rotation. *Agric. For. Meteorol.* **276–277**, 107636 (2019).
8. Drury, C. F. et al. Diverse rotations impact microbial processes, seasonality and overall nitrous oxide emissions from soils. *Soil Sci. Soc. Am. J.* **85**, 1448–1464 (2021).
9. Johnson, J. M. F., Weyers, S. L., Archer, D. W. & Barbour, N. W. Nitrous oxide, methane emission, and yield-scaled emission from organically and conventionally managed systems. *Soil Sci. Soc. Am. J.* **76**, 1347–1357 (2012).
10. Savage, K., Phillips, R. & Davidson, E. High temporal frequency measurements of greenhouse gas emissions from soils. *Biogeosciences* **11**, 2709–2720 (2014).
11. Firestone, M. K. & Davidson, E. A. Microbiologial basis of NO and N2O production and consumption in soil. *Exch. Trace Gas. Terr. Ecosyst. Atmos.* 7–21 https://doi.org/10.1017/CBO9781107415324.004 (1989).
12. Anthony, T. L. & Silver, W. L. Hot moments drive extreme nitrous oxide and methane emissions from agricultural peatlands. *Glob. Chang. Biol.* 15802. https://doi.org/10.1111/gcb.15802 (2021).
13. Bauder, J. W., Jacobsen, J. S. & Lanier, W. T. Alfalfa emergence and survival response to irrigation water quality and soil series. *Soil Sci. Soc. Am. J.* **56**, 890–896 (1992).
14. Davidson, E. A., Keller, M., Erickson, H. E., Verchot, L. V. & Veldkamp, E. Testing a conceptual model of soil emissions of nitrous and nitric oxides. *BioScience* **50**, 667 (2000).
15. Giles, M., Morley, N., Baggs, E. M. & Daniell, T. J. Soil nitrate reducing processes - Drivers, mechanisms for spatial variation, and significance for nitrous oxide production. *Front. Microbiol.* **3**, 1–16 (2012).
16. Sturtevant, C. et al. Identifying scale-emergent, nonlinear, asynchronous processes of wetland methane exchange. *J. Geophys. Res. Biogeosci.* 188–204. https://doi.org/10.1002/2015JG003054.Received (2016).

17. Borken, W. & Matzner, E. Reappraisal of drying and wetting effects on C and N mineralization and fluxes in soils. *Glob. Chang. Biol.* **15**, 808–824 (2009).

18. Canarini, A., Kiær, L. P. & Dijkstra, F. A. Soil carbon loss regulated by drought intensity and available substrate: a meta-analysis. *Soil Biol. Biochem.* **112**, 90–99 (2017).

19. Kim, D. G., Vargas, R., Bond-Lamberty, B. & Turetsky, M. R. Effects of soil rewetting and thawing on soil gas fluxes: a review of current literature and suggestions for future research. *Biogeosciences* **9**, 2459–2483 (2012).

20. Barnard, R. L., Blazewicz, S. J. & Firestone, M. K. Rewetting of soil: revisiting the origin of soil CO2 emissions. *Soil Biol. Biochem.* **147**, 107819 (2020).

21. Leon, E. et al. Hot spots, hot moments, and spatio-temporal controls on soil CO2efflux in a water-limited ecosystem. *Soil Biol. Biochem.* **77**, 12–21 (2014).

22. Davidson, E. A., Janssens, I. A. & Lou, Y. On the variability of respiration in terrestrial ecosystems: moving beyond Q10. *Glob. Chang. Biol.* **12**, 154–164 (2006).

23. Hatala, J. A. et al. Greenhouse gas (CO2, CH4, H2O) fluxes from drained and flooded agricultural peatlands in the Sacramento-San Joaquin Delta. *Agric. Ecosyst. Environ.* **150**, 1–18 (2012).

24. Keane, B. J. et al. Greenhouse gas emissions from the energy crop oilseed rape (Brassica napus); the role of photosynthetically active radiation in diurnal N2O flux variation. *GCB Bioenergy* **10**, 306–319 (2018).

25. Panchal, P., Preece, C., Peñuelas, J. & Giri, J. Soil carbon sequestration by root exudates. *Trends Plant Sci.* **27**, 749–757 (2022).

26. Guyonnet, J. P., Cantarel, A. A. M., Simon, L. & Haichar, F. E. Z. Root exudation rate as functional trait involved in plant nutrient-use strategy classification. *Ecol. Evol.* **8**, 8573–8581 (2018).

27. Haichar, F. et al. Plant host habitat and root exudates shape soil bacterial community structure. *ISME J.* **2**, 1221–1230 (2008).

28. Baldocchi, D. D. et al. Outgoing near-infrared radiation from vegetation scales with canopy photosynthesis across a spectrum of function, structure, physiological capacity, and weather. *J. Geophys. Res. Biogeosci.* **125**, e2019JG005534 (2020).

29. Oikawa, P. Y. et al. Evaluation of a hierarchy of models reveals importance of substrate limitation for predicting carbon dioxide and methane exchange in restored wetlands. *J. Geophys. Res. Biogeosci.* **122**, 145–167 (2017).

30. Serrano-Silva, N., Sarria-Guzmàn, Y., Dendooven, L. & Luna-Guido, M. Methanogenesis and methanotrophy in soil: a review. *Pedosphere* **24**, 291–307 (2014).

31. Hemes, K. S. et al. Assessing the carbon and climate benefit of restoring degraded agricultural peat soils to managed wetlands. *Agric. For. Meteorol.* **268**, 202–214 (2019).

32. Sapkota, A., Haghverdi, A., Avila, C. C. E. & Ying, S. C. Irrigation and greenhouse gas emissions: a review of field-based studies. *Soil Syst.* **4**, 20 (2020).

33. Speight, J. G. 5 - Sources of water pollution. in *Natural Water Remediation* (ed. Speight, J. G.) 165–198 (Butterworth-Heinemann, 2020). https://doi.org/10.1016/B978-0-12-803810-9.00005-X.

34. Rochette, P. et al. Emissions of N2O from alfalfa and soybean crops in Eastern Canada. *Soil Sci. Soc. Am. J.* **68**, 493–506 (2004).

35. Wagner-Riddle, C., Thurtell, G. W., Kidd, G. K., Beauchamp, E. G. & Sweetman, R. Estimates of nitrous oxide emissions from agricultural fields over 28 months. *Can. J. Soil Sci.* **77**, 135–144 (1997).

36. Burger, M., Haden, V. R., Chen, H., Six, J. & Horwath, W. R. Stand age affects emissions of N2O in flood-irrigated alfalfa: a comparison of field measurements, DNDC model simulations and IPCC Tier 1 estimates. *Nutr. Cycl. Agroecosyst.* **106**, 335–345 (2016).

37. Mosier, A. R., Halvorson, A. D., Peterson, G. A., Robertson, G. P. & Sherrod, L. Measurement of net global warming potential in three agroecosystems. *Nutr. Cycl. Agroecosyst.* **72**, 67–76 (2005).

38. Deng, J. et al. Changes in irrigation practices likely mitigate nitrous oxide emissions from California cropland. *Glob. Biogeochem. Cycles* **32**, 1514–1527 (2018).

39. Syakila, A. & Kroeze, C. The global nitrous oxide budget revisited. *Greenh. Gas Meas. Manag.* **1**, 17–26 (2011).

40. Robertson, G. P., Paul, E. A. & Harwood, R. R. Greenhouse gases in intensive agriculture: contributions of individual gases to the radiative forcing of the atmosphere. *Science* **289**, 1922–1925 (2000).

41. Snyder, C. S., Bruulsema, T. W., Jensen, T. L. & Fixen, P. E. Review of greenhouse gas emissions from crop production systems and fertilizer management effects. *Agric. Ecosyst. Environ.* **133**, 247–266 (2009).

42. Shouse, P. J., Ayars, J. E. & Šimůnek, J. Simulating root water uptake from a shallow saline groundwater resource. *Agric. Water Manag.* **98**, 784–790 (2011).

43. Kandelous, M. M. et al. Evaluation of subsurface drip irrigation design and management parameters for alfalfa. *Agric. Water Manag.* **109**, 81–93 (2012).

44. Noory, H., Liaghat, A. M., Chaichi, M. R. & Parsinejad, M. Effects of water table management on soil salinity and alfalfa yield in a semi-arid climate. *Irrig. Sci.* **27**, 401–407 (2009).

45. Orchard, V. A. & Cook, F. J. Relationship between soil respiration and soil moisture. *Soil Biol. Biochem.* **15**, 447–453 (1983).

46. Moran, J. F. et al. Drought induces oxidative stress in pea plants. *Planta* **194**, 346–352 (1994).

47. Tang, L. et al. Overexpression of GsZFP1 enhances salt and drought tolerance in transgenic alfalfa (Medicago sativa L.). *Plant Physiol. Biochem.* **71**, 22–30 (2013).

48. Shaaban, M. et al. Reduction in soil N2O emissions by pH manipulation and enhanced nosZ gene transcription under different water regimes. *Environm. Poll.* **235**, 625–631 (2018).

49. Anthony, T. L. & Silver, W. L. Mineralogical associations with soil carbon in managed wetland soils. *Glob. Chang Biol.* **26**, 6555–6567 (2020).

50. Krichels, A. H. & Yang, W. H. Dynamic controls on field-scale soil nitrous oxide hot spots and hot moments across a microtopographic gradient. *J. Geophys. Res. Biogeosci.* **124**, 3618–3634 (2019).

51. Kavdır, Y., Rasse, D. P. & Smucker, A. J. M. Specific contributions of decaying alfalfa roots to nitrate leaching in a Kalamazoo loam soil. *Agric. Ecosys. Environ.* **109**, 97–106 (2005).

52. Burity, H. A., Ta, T. C., Faris, M. A. & Coulman, B. E. Estimation of nitrogen fixation and transfer from alfalfa to associated grasses in mixed swards under field conditions. *Plant Soil* **114**, 249–255 (1989).

53. Thilakarathna, M. S., McElroy, M. S., Chapagain, T., Papadopoulos, Y. A. & Raizada, M. N. Belowground nitrogen transfer from legumes to non-legumes under managed herbaceous cropping systems. A review. *Agron. Sustain. Dev.* **36**, 1–16 (2016).

54. Brophy, L. S. & Heichel, G. H. Nitrogen release from roots of alfalfa and soybean grown in sand culture. *Plant Soil* **116**, 77–84 (1989).

55. Erice, G. et al. Photosynthesis, N2 fixation and taproot reserves during the cutting regrowth cycle of alfalfa under elevated CO2 and temperature. *J. Plant Physiol.* **168**, 2007–2014 (2011).

56. Ning, J. et al. Optimizing alfalfa productivity and persistence versus greenhouse gases fluxes in a continental arid region. *PeerJ* **2020**, 1–19 (2020).

57. Conrad, R. Soil microorganisms as controllers of atmospheric trace gases (H2, CO, CH4, OCS, N2O, and NO). *Microbiol. Rev.* **60**, 609–640 (1996).

58. Kammann, C., Hepp, S., Lenhart, K. & Müller, C. Stimulation of methane consumption by endogenous CH4 production in aerobic grassland soil. *Soil Biol. Biochem.* **41**, 622–629 (2009).

59. Bender, M. & Conrad, R. Methane oxidation activity in various soils and freshwater sediments: Occurrence, characteristics, vertical profiles, and distribution on grain size fractions. *J. Geophys. Res.* **99**, 16531 (1994).

60. Min, K. et al. Differential effects of wetting and drying on soil CO2 concentration and flux in near-surface vs. deep soil layers. *Biogeochemistry* **7**, 255–269 (2020).

61. Von Fischer, J. C., Butters, G., Duchateau, P. C., Thelwell, R. J. & Siller, R. In situ measures of methanotroph activity in upland soils: A reaction diffusion model and field observation of water stress. *J. Geophys. Res. Biogeosci.* **114**, 1–12 (2009).

62. O'neill, J. G. & Wilkinson, J. F. Oxidation of ammonia by methane-oxidizing bacteria and the effects of ammonia on methane oxidation. *Microbiology* **100**, 407–412 (1977).

63. Yoshinari, T. Nitrite and nitrous oxide production by Methylosinus trichosporium. *Can. J. Microbiol.* **31**, 139–144 (1985).

64. Jones, R. D. & Morita, R. Y. Methane oxidation by Nitrosococcus oceanus and Nitrosomonas europaea. *Appl. Environ. Microbiol.* **45**, 401–410 (1983).

65. Ward, B. B. Kinetic studies on ammonia and methane oxidation by Nitrosococcus oceanus. *Arch. Microbiol.* **147**, 126–133 (1987).

66. Hassanat, F., Gervais, R., Massé, D. I., Petit, H. V. & Benchaar, C. Methane production, nutrient digestion, ruminal fermentation, N balance, and milk production of cows fed timothy silage- or alfalfa silage-based diets. *J. Dairy Sci.* **97**, 6463–6474 (2014).

67. Schmitt, A., Pausch, J. & Kuzyakov, Y. C and N allocation in soil under ryegrass and alfalfa estimated by 13C and 15N labelling. *Plant Soil* **368**, 581–590 (2013).

68. Schmitt, A., Pausch, J. & Kuzyakov, Y. Effect of clipping and shading on C allocation and fluxes in soil under ryegrass and alfalfa estimated by 14C labelling. *Appl. Soil Ecol.* **64**, 228–236 (2013).

69. Lambers, H., Raven, J. A., Shaver, G. R. & Smith, S. E. Plant nutrient-acquisition strategies change with soil age. *Trends Ecol. Evol.* **23**, 95–103 (2008).

70. The Delta Protection Commission. The State of Delta Agriculture: Economic Impact, Conservation and Trends. (2020).

71. Putnam, D. H., Summers, C. G. Orloff, S. B. Alfalfa production systems in California. in *Irrigated alfalfa management for Mediterranean and Desert zones* (University of California Agriculture and Natural Resources, 2007).

72. Camilo, R.-S., Szutu, D., Baldocchi, D. & Hemes, K. meriFlux BASE US-Bi2 Bouldin Island corn, Ver. 13-5, AmeriFlux AMP, (Dataset). https://doi.org/10.17190/AMF/1419513 (2021).

73. PlanetTeam. Planet Application Program Interface: In *Space for Life on Earth*. https://api.planet.com (2021).

74. Houborg, R. & McCabe, M. F. High-Resolution NDVI from planet's constellation of earth observing nano-satellites: a new data source for precision agriculture. *Remote Sens.* **8**, 768 (2016).

75. Kong, J. et al. Matching high resolution satellite data and flux tower footprints improves their agreement in photosynthesis estimates. *Agric. For. Meteorol.* **316**, 108878 (2022).

76. Soil Survey Staff. Natural Resources Conservation Service, United States Department of Agriculture. *Official Soil Series Descriptions*. (2020). Available at: https://www.nrcs.usda.gov/resources/data-and-reports/web-soil-survey#citation. Accessed [June/08/2020].

77. Nickerson, N. Evaluating gas emission measurements using Minimum Detectable Flux (MDF). *White Paper* (2016).

78. O'Connell, C. S., Ruan, L. & Silver, W. L. Drought drives rapid shifts in tropical rainforest soil biogeochemistry and greenhouse gas emissions. *Nat. Commun.* **9**, 1348 (2018).

79. Baldocchi, D. D., Hicks, B. B. & Meyers, T. P. Measuring biosphere-atmosphere exchanges of biologically related gases with micrometeorological methods. *Ecology* **69**, 1331–1340 (1988).

80. Eichelmann, E. et al. The effect of land cover type and structure on evapotranspiration from agricultural and wetland sites in the Sacramento/San Joaquin River Delta, California. *Agric. For. Meteorol.* **256–257**, 179–195 (2018).

81. Myhre, G. et al. Anthropogenic and natural radiative forcing. *Climate Change 2013: The Physical Science Basis. Contribution of Working Group I to the Fifth Assessment Report of the Intergovernmental Panel on Climate Change* 659–740 https://doi.org/10.1017/CBO9781107415324.018 (2013).

82. Benhadi-Marín, J. A conceptual framework to deal with outliers in ecology. *Biodivers. Conserv.* **27**, 3295–3300 (2018).

83. Hart, S. C., Stark, J. M., Davidson, E. A. & Firestone, M. K. Nitrogen mineralization, immobilization, and nitrification. in *Methods of Soil Analysis, Part 2. Microbial and Biochemical Properties* (eds. Weaver, R. W., Angle, J. S. & Bottomley, P. S.) 985–1018 (Soil Science Society of America, 1994).

84. McLean, E. O. Soil pH and Lime Requirement. in *Page, A.L., Ed., Methods of Soil Analysis. Part 2. Chemical and Microbiological Properties, American Society of Agronomy, Soil Science Society of America, Madison,* 199–224 (1982).

85. Liu, P. C. Wavelet spectrum analysis and ocean wind waves. in *Wavelets in Geophysics* (eds. Foufoula-Georgiou, E. & Kumar, P. B. T.-W. A. and I. A.) vol. **4** 151–166 (Academic Press, 1994).

86. Wood, T. E., Detto, M. & Silver, W. L. Sensitivity of soil respiration to variability in soil moisture and temperature in a humid tropical forest. *PLoS One* **8**, e80965 (2013).

87. Rodríguez-Murillo, J. C. & Filella, M. Significance and causality in continuous wavelet and wavelet coherence spectra applied to hydrological time series. *Hydrology* **7**, 82 (2020).

88. Rösch, A. & Schmidbauer, H. WaveletComp: Computational Wavelet Analysis. R package version 1.1. 1–38 (2018).

89. Mondal, D. & Percival, D. B. Wavelet variance analysis for gappy time series. *Ann. Inst. Stat. Math.* **62**, 943–966 (2010).

Author contributions
T.L.A. wrote the original draft and created the visualizations, W.L.S. and D.D.B. conducted reviews and editing of the original draft, T.L.A. and W.L.S. conceptualized the paper, T.L.A., W.L.S., D.D.B., J.G.V., and D.J.S. contributed to the methodology and data investigation.

Competing interests
The authors declare no competing interests.

Additional information

Supplementary information The online version contains supplementary material available at https://doi.org/10.1038/s41467-023-37391-2.

Correspondence and requests for materials should be addressed to Tyler L. Anthony.

Peer review information *Nature Communications* thanks the other anonymous reviewer(s) for their contribution to the peer review of this work. Peer review reports are available.

Reprints and permissions information is available at http://www.nature.com/reprints

Publisher's note Springer Nature remains neutral with regard to jurisdictional claims in published maps and institutional affiliations.